ELSEVIER

26 April 1996

Chemical Physics Letters 253 (1996) 1–7

CHEMICAL PHYSICS LETTERS

Efficient parallel implementation of response theory: calculations of the second hyperpolarizability of polyacenes

P. Norman [a], D. Jonsson [a], H. Ågren [a], P. Dahle [b], K. Ruud [b], T. Helgaker [b], H. Koch [c]

[a] *Institute of Physics and Measurement Technology, Linköping University, S-58183, Linköping, Sweden*
[b] *Department of Chemistry, University of Oslo, Box 1033, Blindern, N-0315 Oslo, Norway*
[c] *Department of Chemistry, Aarhus University, DK-8000 Århus C, Denmark*

Received 3 January 1996; in final form 19 February 1996

Abstract

We describe an efficient parallel implementation of response theory for calculations of molecular properties, and demonstrate its performance by calculations on a series of polyacene molecules, from benzene to hexacene. The polarizability and the second hyperpolarizability of the molecules in this series are found to scale as $N^{1.4}$ and $N^{3.5}$, respectively, where N is the number of benzene rings in the molecule. These N-dependences are weaker than those predicted for the linear polyenes.

1. Introduction

There has recently been an intense search for molecules with large non-linear properties and with technical applicability as constituents in optically active materials. An introduction to this field is given in the review article by Brédas et al. [1]. The important role played by theoretical calculations in this search has been increasingly acknowledged. Computer simulations can make it possible to screen candidate compounds, thereby avoiding expensive experimental tests. In addition to predicting properties, simulations may provide understanding in terms of special structure-to-property relationships, which in turn can help design better and more efficient laboratory tests.

Much theoretical work has been devoted to linear conjugated systems for which the size dependence of non-linear response and the relationship between the optical properties and electronic and geometrical structure parameters have been of special interest. Although the gap in size between systems that are manageable for theoretical investigations and those of technical interest has been narrowing, the applicability of ab initio calculations of non-linear optical responses is still restricted by the rather large basis sets needed. Because of the size of the constituting units, the polyacenes belong to the category of interesting systems, which, except for the first three members, have been out of the reach of ab initio calculations of its non-linear properties. This is unfortunate from the point of view that many promising optically active materials contain benzene rings as building blocks, often connected by special bridge units and terminated by groups of donor/acceptor character. It is therefore desirable to investigate further the polyacenes as model compounds and compare, for example, with the linear polyenes for which

PII S0009-2614(96)00246-1

a great deal has already been learned; see, for instance, Refs. [2–5].

The development of ab initio methods is driven by, on one hand, theoretical improvements and, on the other hand, the development of more powerful computing resources. Thus by combining direct methods with parallel computing, we not only avoid the bottleneck of disk space but also drastically improve the speed of large-scale calculations. It is our purpose to present this technique by calculating the polarizability and second hyperpolarizability at the RPA (random phase approximation) level for the first six members of the linear polyacenes: benzene, naphthalene, anthracene, naphthacene, pentacene, and hexacene. As these molecules all belong to the D_{2h} point group, the first hyperpolarizability vanishes.

2. Method

2.1. Fock matrices in a response calculation

Following the general response formalism introduced in the work by Olsen and Jørgensen [6], an extension to third-order responses of the system to perturbing fields has recently been formulated [7]. Using an SCF reference state, in this terminology, our method is coined the cubic random phase approximation (CRPA). A primary example among the new applications reached by this theory on a fully analytical level is the second hyperpolarizability that can be identified as minus the value of the cubic response function for dipole operators. However, many other molecular properties, both electric and magnetic, are also embraced with no other effort than a mere substitution of the operators.

The final computational expression for the third-order response function is rather complex and lengthy, containing a set of coupled linear equations to be solved for seven response vectors followed by contractions of multiple-indexed matrices. From a computational point of view, the contraction of a fourth-order Hessian matrix with three response vectors is the most crucial and a simplistic implementation would limit the applicability to small systems. We have therefore included direct strategies both in terms of multiple one-index transformations as well as two-electron integral evaluation and can thereby perform fourth-order property calculations on systems of the same size as in direct SCF [7].

Comparing the expressions for the linear and the cubic response function given in Ref. [7], one sees that the corresponding first-order response property, in this case the polarizability, can be obtained at no extra cost as an inner product between a response vector and a first-order property matrix. On the other hand, the excitation energies of the system are identified as the residues of the linear response function and therefore require the solution of an additional eigenvalue problem.

Both the wavefunction optimization, using SCF gradients, as well as the subsequent response calculation, with all its matrix contractions, can be expressed in terms of transformed inactive Fock matrices. The computationally intensive part is thus localized to the construction of these Fock matrices, and this localization favors parallelization, as will be discussed below.

The large number of two-electron integrals prohibits a strategy where the two-electron integrals are calculated in advance and stored on disk. Instead, the necessary Fock matrices are instead constructed from atomic integrals calculated on the fly. Denoting inactive MO's with j, general MO's with p, q, r, s and AO's with Greek letters, we have

$$F_{rs} = h_{rs} + \mathscr{G}_{rsjj}, \tag{1}$$

$$\mathscr{G}_{rsjj} = 2(rs\,|\,jj) - (rj\,|\,js). \tag{2}$$

The Fock matrix calculated from one-index transformed integrals take the form

$$\bar{F}_{rs} = \bar{h}_{rs} + \bar{\mathscr{G}}_{rsjj}, \tag{3}$$

$$\bar{h}_{rs} = {}^1\kappa_{rp} h_{ps} - {}^1\kappa_{ps} h_{rp}, \tag{4}$$

$$\bar{\mathscr{G}}_{rspj} = {}^1\kappa_{rq}\mathscr{G}_{qspj} - {}^1\kappa_{qs}\mathscr{G}_{rqpj} + {}^1\kappa_{pq}\mathscr{G}_{rsqj} - {}^1\kappa_{qj}\mathscr{G}_{rspq}. \tag{5}$$

Using Eqs. (3), (4) and (5) repeatedly, we obtain after expanding $\mathscr{G}$ in atomic orbitals

$$\bar{\mathbf{F}} = [{}^1\boldsymbol{\kappa}, \mathbf{F}] + \mathbf{F}^1, \tag{6}$$

$$\bar{\bar{\mathbf{F}}} = \left[{}^1\boldsymbol{\kappa}, \left[{}^2\boldsymbol{\kappa}, \mathbf{F}\right] + 2\mathbf{F}^2\right] + \left[{}^2\boldsymbol{\kappa}, \left[{}^1\boldsymbol{\kappa}, \mathbf{F}\right] + 2\mathbf{F}^1\right] + \mathbf{F}^{(12)}, \tag{7}$$

$$\begin{aligned}\tilde{\tilde{\mathbf{F}}} = &\left[{}^{1}\boldsymbol{\kappa}, \left[{}^{2}\boldsymbol{\kappa}, \left[{}^{3}\boldsymbol{\kappa}, \mathbf{F}\right] + 3\mathbf{F}^{3}\right]\right] \\ &+ \left[{}^{3}\boldsymbol{\kappa}, \left[{}^{2}\boldsymbol{\kappa}, \mathbf{F}\right] + 3\mathbf{F}^{2}\right] + 3\mathbf{F}^{(23)}\right] \\ &+ \left[{}^{2}\boldsymbol{\kappa}, \left[{}^{1}\boldsymbol{\kappa}, \left[{}^{3}\boldsymbol{\kappa}, \mathbf{F}\right] + 3\mathbf{F}^{3}\right]\right] \\ &+ \left[{}^{3}\boldsymbol{\kappa}, \left[{}^{1}\boldsymbol{\kappa}, \mathbf{F}\right] + 3\mathbf{F}^{1}\right] + 3\mathbf{F}^{(13)}\right] \\ &+ \left[{}^{3}\boldsymbol{\kappa}, \left[{}^{2}\boldsymbol{\kappa}, \left[{}^{1}\boldsymbol{\kappa}, \mathbf{F}\right] + 3\mathbf{F}^{1}\right]\right] \\ &+ \left[{}^{1}\boldsymbol{\kappa}, \left[{}^{2}\boldsymbol{\kappa}, \mathbf{F}\right] + 3\mathbf{F}^{2}\right] + 3\mathbf{F}^{(12)}\right] \\ &+ \mathbf{F}^{(123)}, \end{aligned} \tag{8}$$

where the intermediate Fock matrices and the density matrices needed for their construction are given by

$$F^{123}_{rs} = D^{123}_{\alpha\beta}\mathscr{L}_{rs\alpha\beta}, \tag{9}$$

$$\begin{aligned}D^{123}_{\alpha\beta} = &{}^{1}\kappa_{jp}\,{}^{2}\kappa_{pq}\,{}^{3}\kappa_{qt}c_{\alpha t}c_{\beta j} - {}^{1}\kappa_{jp}\,{}^{2}\kappa_{pq}\,{}^{3}\kappa_{tj}c_{\alpha q}c_{\beta t} \\ &- {}^{1}\kappa_{jp}\,{}^{2}\kappa_{qj}\,{}^{3}\kappa_{pt}c_{\alpha t}c_{\beta q} + {}^{1}\kappa_{jp}\,{}^{2}\kappa_{qj}\,{}^{3}\kappa_{tq}c_{\alpha p}c_{\beta t} \\ &- {}^{1}\kappa_{pj}\,{}^{2}\kappa_{jq}\,{}^{3}\kappa_{qt}c_{\alpha t}c_{\beta p} + {}^{1}\kappa_{pj}\,{}^{2}\kappa_{jq}\,{}^{3}\kappa_{tp}c_{\alpha q}c_{\beta t} \\ &+ {}^{1}\kappa_{pj}\,{}^{2}\kappa_{qp}\,{}^{3}\kappa_{jt}c_{\alpha t}c_{\beta q} - {}^{1}\kappa_{pj}\,{}^{2}\kappa_{qp}\,{}^{3}\kappa_{tq}c_{\alpha j}c_{\beta t}, \end{aligned} \tag{10}$$

$$F^{mn}_{rs} = D^{mn}_{\alpha\beta}\mathscr{L}_{rs\alpha\beta}, \tag{11}$$

$$\begin{aligned}D^{mn}_{\alpha\beta} = &{}^{m}\kappa_{jp}\,{}^{n}\kappa_{pq}c_{\alpha q}c_{\beta j} - {}^{m}\kappa_{jp}\,{}^{n}\kappa_{qj}c_{\alpha p}c_{\beta q} \\ &- {}^{m}\kappa_{pj}\,{}^{n}\kappa_{jq}c_{\alpha q}c_{\beta p} + {}^{m}\kappa_{pj}\,{}^{n}\kappa_{qp}c_{\alpha j}c_{\beta q}, \end{aligned} \tag{12}$$

$$F^{m}_{rs} = D^{m}_{\alpha\beta}\mathscr{L}_{rs\alpha\beta}, \tag{13}$$

$$D^{m}_{\alpha\beta} = {}^{m}\kappa_{jp}c_{\alpha p}c_{\beta j} - {}^{m}\kappa_{pj}c_{\alpha j}c_{\beta p}. \tag{14}$$

We refer to Ref. [7] for the expressions in which these Fock matrices appear.

We notice the relatively large number of Fock matrices needed to obtain the cubic response function. In addition, each Fock matrix F^m is re-evaluated repeatedly during the optimization of the wavefunction and the iterative solution of the response equations. In the next section we describe how we may parallelize the construction of these Fock matrices.

2.2. Parallel implementation of cubic response functions

A simple but efficient strategy for the parallelization of the Fock matrix construction has been presented in Ref. [8], and the same philosophy is adopted here. All the Fock matrices in Eqs. (1)–(8) are parallelized by distributing the computation of the two-electron integrals on different nodes, and constructing the parts of the Fock matrix that these integrals contribute to on each individual machine. When all two-electron integrals have been evaluated, the contributions to the Fock matrix are collected from the different machines and added to the one-electron contribution. This strategy implies that we must distribute the density matrix to all nodes, and keep a local matrix of the same size as the Fock matrix on each node.

In our program, we group atomic orbitals at different levels. All basis functions with the same angular momentum and exponents on a single symmetry-independent atomic center are denoted a shell, and all shells with a given angular momentum (but possibly different exponents) are collectively denoted a block of shells. The two-electron integrals are calculated in batches, the batch being defined as all integrals resulting from the block of shells i, j, k and l, and we will implicitly assume this batch of integrals from the notation $(ij|kl)$ (Mulliken notation) for the two-electron integrals. To reduce the communication to computation ratio, we distribute all two-electron integrals of the same overlap distributions $(ij|$ to the same node. Thus, for a given $(ij|$, $i \geqslant j$, we compute on one computer the batch groups of integrals

$$(ij|kl)\forall k,\ l \quad l \leqslant k < i,\ l \leqslant j \text{ for } k = 1. \tag{15}$$

This scheme gives a smaller communication to computation ratio than, for instance, the implementation described in Ref. [8] and also avoids distributing too small tasks. The program exploits D_{2h} symmetry, but there is currently no integral pre-screening implemented.

We have given a schematic overview of our implementation in Table 1, which may be compared to Table 2 of Ref. [8]. For simplicity we have ignored the treatment of symmetry in Table 1. As in Ref. [8] we have employed a master/slave paradigm in order to exploit dynamical load balancing, yet implementing this so as to obtain a single program multiple data (SPMD) structure. The distribution of tasks is carried out as follows: in the construction of the first Fock matrix, tasks are distributed to a slave

as soon as it becomes available, and the time on each task is recorded. The list of timings is then sorted and used in all subsequent Fock matrix constructions, where the most time-consuming tasks are distributed first. In this way we avoid the distribution of large tasks at late stages of the Fock matrix construction which would lead to large idle time for the rest of the slaves.

The localized structure of the parallelization makes it easy to implement in existing ab initio codes, and we have implemented this approach in the DALTON program [9]. This program consists of more than 1700 subroutines, but the changes needed for the parallelization are localized to less than 25 of these. Furthermore, the amount of communication is reduced to a minimum, being restricted to sending the density matrix and the shell-indices from the master to the slaves, and return the Fock matrix from the slaves back to the master. The drawback of the implementation is memory requirements. As the master and each slave need to have a local copy of the Fock and density matrices during the calculation, the memory requirements for each node is the same as for sequential calculations. However, as clusters of workstations with large local memory are becoming more widespread for parallelization, we do not consider this to be a serious drawback at the present.

Table 1
Structure of the parallel implementation of the construction of the Fock matrices

Master code	
a	Send density matrix to all slaves
b	Loop over index i
c	Loop over index $j \leqslant i$
d	Send indexes i and j to an idle slave
e	End of loops
f	Collect all contributions to **F** from all slaves
h	Symmetrize **F** and and one-electron contributions
g	Sort integral timings
Slave code	
a	Collect **D** from master and zero **F**
b	Receive shell indexes i and j
c	Loop over all $k \leqslant i$
d	Loop over all $l \leqslant k$ (or $l \leqslant j$ if $i = k$)
e	Compute $(ij \mid kl)$
f	Add integral $(ij \mid kl)$ to **F**
g	End of loops
h	If more to do on this Fock matrix, goto b, else goto a

Table 2
Parallel efficiency

# rings	# nodes	Slave efficiency	Total efficiency	Theoretical
1	9	98.5	85.2	88.9
2	8	99.1	86.8	87.5
3	9	99.0	87.5	88.9
4	8	99.1	86.5	87.5
5	8	99.2	86.6	87.5
6	10	98.9	88.8	90.0

The number of nodes is the total number of nodes (including the master), and the number of slaves is this number minus one.

The above parallelization strategy has been implemented using both PVM3 and MPI as message passing interfaces, and the program has been ported to the IBM-SP2, Intel Paragon, Cray-T3D, SGI-PowerChallenge and a heterogeneous cluster of IBM workstations. We performed calculations on two different IBM-RS6000/SP2 clusters located in Oslo and Stockholm with 16 and 55 nodes, respectively, using MPI for message passing. However, in order to give a unified comparison of the efficiency, all timings reported here are from the SP2 cluster in Oslo. By efficiency we here refer to the ratio of CPU time to wall time (giving an effective number of computers) compared to the number of computers used in the calculation. The number of nodes is allocated automatically by the queue system and is reported in Table 2. Note that due to the switch on the SP2s (we cannot start a slave on the master machine), the maximum efficiency will be (with no time spent in the sequential parts)

$$\text{Maximum efficiency} = \frac{(\text{number of nodes} - 1) \times 100\%}{(\text{number of nodes})}. \tag{16}$$

Thus we report in Table 2 both the efficiency in the purely parallel parts of the calculation, given with respect to the number of slaves, and the overall efficiency given with respect to the total number of nodes. A more detailed investigation of the general scalability of the approach presented here will be given elsewhere.

3. Computations

3.1. Basis set and geometries

The choice of a basis set for hyperpolarizability calculations is crucial. Extensive basis set investigations have already been performed for many organic molecules. Accurate RPA values for hyperpolarizabilities have been obtained using a 4-31G basis set [10,11] with additional polarizing and diffuse p- and d-functions on the carbons, both with an exponent of 0.05. For the benzene molecule this basis set generates 114 basis functions. For each additional benzene unit 72 basis functions are introduced, giving a total of 474 basis functions for hexacene. As the number of basis functions grows larger, the numerical threshold for linear dependence becomes important. The actual number of molecular orbitals in the wavefunction optimization will thus be somewhat smaller than the total number of basis functions. For instance, hexacene was optimized with only 451 molecular orbitals, even though the basis set consists of 474 basis functions.

The following geometries were used: C–C distances of 1.399 and 1.401 Å for benzene and naphthalene, respectively, and anthracene according to Fig. 1. Based on these structures, the geometries for the longer polyacenes were constructed; naphthacene and pentacene by additional mid-units to anthracene, and hexacene by additional naphthalene units to each end of naphthacene.

3.2. Results

We have chosen the x-axis to serve as the polymeric in-plane long-axis and consequently focus our attention on the xx and $xxxx$ components of the polarizability and second hyperpolarizability, respectively, as this direction will become increasingly more dominating as the chain length becomes larger. Ab initio calculations of the polarizability for the three shortest molecules, benzene, naphthalene, and anthracene [12–14], and of the second hyperpolarizability for benzene [14] are available in the literature. Semi-empirical calculations of both the polarizability and the second hyperpolarizability exist for all molecules investigated here [15].

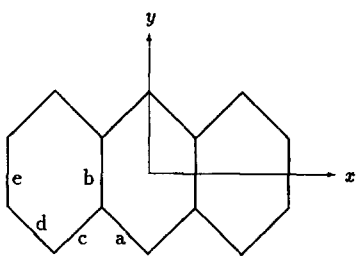

Fig. 1. Anthracene geometry in Å: (a) 1.396, (b) 1.436, (c) 1.423, (d) 1.371, (e) 1.408

Polarizabilities for benzene close to the HF limit have been reported by Lazzaretti et al. [16]. Our value of 76.9 au, see Table 4, for benzene is within 2% of the results obtained with their largest basis set, giving further support for our choice of basis set. Perrin et al. [14] calculated the polarizability and hyperpolarizability of benzene using the same basis set as we have employed [11] using analytical expressions for the SCF energy derivatives with respect to the electric field. The two methods, although different in formulation, should give identical results and the deviation between our values ($\alpha_{xx} = 76.95$ au, $\gamma_{xxxx} = 1.424 \times 10^4$ au) and their values ($\alpha_{xx} = 74.2$ au, $\gamma_{xxxx} = 1.411 \times 10^4$ au) must be ascribed to geometry differences, indicating a fairly strong geometry dependence of the properties.

Hinchliffe and Machado [13] have performed a coupled perturbed HF calculation of the polarizability of naphthalene for a number of different basis sets. With increasing quality of the basis set they observed an increasing polarizability; their largest basis set value of 150.1 au compares well with our value of 156.8 au. For experimental comparison we refer to a laser Stark spectroscopy experiment by Heitz et al. [17] determining the long in-plane component of the ground state polarizability to 163 au, remarkably close to our value. The most accurate SCF polarizability calculation for anthracene (254 au), given by Perez and Villar [12], is in good agreement with our value of 260 au. Both values fall in the middle of a number of experimental results varying from 240 to 291 au [18–22].

For the linear polyacenes, semi-empirical MNDO calculations of up to eight benzene units [15] have predicted a power form dependence between the average polarizabilities, $\langle \alpha \rangle$ and $\langle \gamma \rangle$, and the number of units. Also the band gap has been proposed as

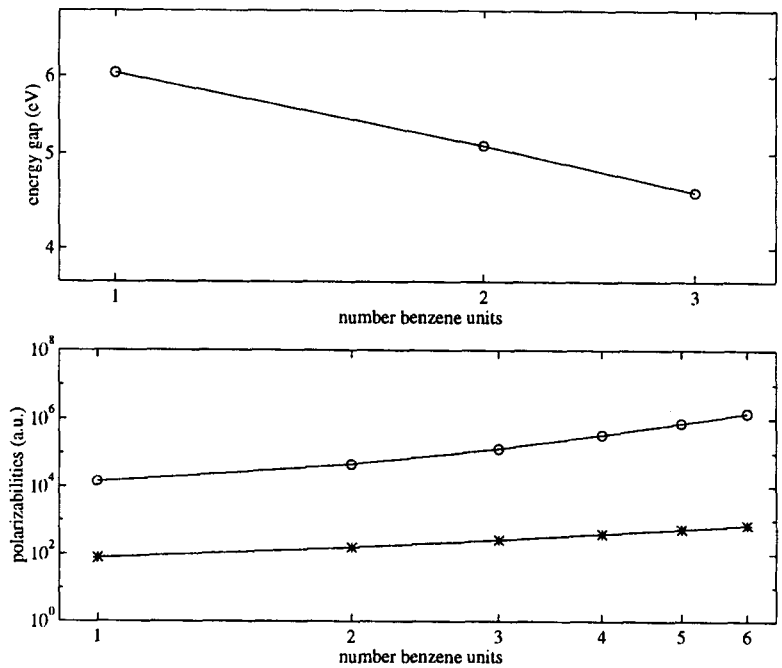

Fig. 2. Properties versus number of benzene units for polyacene: (a) band gap and (b) polarizability (stars), second hyperpolarizability (rings).

a structure parameter. In Fig. 2 we present our results for the polarizability, second hyperpolarizability and energy band gap versus the number of benzene units. Excluding benzene and naphthalene for the second hyperpolarizability we observe that a power form dependence holds for the polarizabilities as well as for the band gap, seen as straight lines in the logarithmic plots. Using smaller polymeric building blocks, such as ethylene units, these length dependences have previously been investigated on an ab initio level, see Refs. [4,5,23,24]. The exponents obtained from the logarithmic fit of the band gap, the polarizability and the second hyperpolarizability to the number of benzene units are collected in Table 3, where they are compared with similar exponents obtained from a recent investigation of ground and excited state polarizabilities of polyenes [25]. The polyene spectra are strongly dominated by the $1A_g \rightarrow 1B_u$ transition, which determines the band gap, and the lowering of the band gap energy with increasing number of ethene units will consequently enhance the polarizability values, see Ref. [5] for details. For the polyacenes, the corresponding long in-plane transition is $1A_g \rightarrow 1B_{3u}$. It is seen that the polyenes show a more rapidly decreasing band gap energy, $E_g \propto N^{-0.40}$, than the polyacenes, $E_g \propto N^{-0.25}$, in agreement with the more rapidly increasing polarizabilities. In Table 4 we have collected our results for the polarizability and hyperpolarizability

Table 3
Exponents of a power form dependence of the band gap and polarizabilities versus the number of polymer units

	E_g	α_{xx}	γ_{xxxx}
Polyacene	−0.25	1.4	3.5
Polyene	−0.4	1.7	4.2

Table 4
Static polarizability (au) and second hyperpolarizability (10^4 au) versus the number of benzene units

	α_{xx} [a]	α_{xx} [b]	γ_{xxxx} [a]
1	76.95	89.10	1.424
2	156.8	180.3	4.644
3	260.3	298.1	13.36
4	389.6	438.1	34.10
5	539.3	596.7	74.74
6	704.6	770.2	144.3

[a] Our values.
[b] MNDO calculation [15].

as well as the MNDO polarizability values of Ref. [15]. The MNDO results overshoot our CRPA results by 10–15% which, however, must be considered to be in fair agreement with our results, and support the use of semi-empirical methods to investigate trends in non-linear properties.

4. Conclusions

We have demonstrated that with an effective parallel implementation of non-linear response theory at the random phase approximation level, calculations of polarizabilities and hyperpolarizabilities can be applied to systems that are sufficiently large to be of technical interest. Apart from directly predicting properties, these calculations make it possible to calibrate trends from already established semi-empirical techniques. The polarizability and the second hyperpolarizability of the molecules in the polyacene series, chosen here for illustration, were found to scale as $N^{1.4}$ and $N^{3.5}$, respectively, where N is the number of benzene units. These scalings are weaker than those predicted for the linear polyenes in terms of ethylene units.

Acknowledgement

This work has received support from the Norwegian Supercomputing Committee (TRU) and the Parallel Data Center (PDC) at the Royal Institute of Technology in Stockholm through grants of computing time.

References

[1] J.L. Brédas, C. Adant, P. Tackx and A. Persoons, Chem. Rev. 94 (1994) 243.
[2] J.K. Hurley, H. Lincshitz and A. Treinin, J. Phys. Chem. 92 (1988) 5151.
[3] S.P. Karna, G.B. Talapatra, W.M.K.P. Wijekoon and P.N. Prasad, Phys. Rev. A 45 (1992) 2763.
[4] B. Champagne, J.G. Fripiat and J.-M. Andre, J. Chem. Phys. 96 (1992) 8330.
[5] Y. Luo, H. Ågren, H. Koch, P. Jørgensen and T. Helgaker, Phys. Rev. B 51 (1995) 14949.
[6] J. Olsen and P. Jørgensen, J. Chem. Phys. 82 (1985) 3235.
[7] P. Norman, D. Jonsson, O. Vahtras and H. Ågren, Chem. Phys. Letters 242 (1995) 7.
[8] M. Feyereisen and R.A. Kendall,. Theoret. Chim. Acta 84 (1993) 289.
[9] T. Helgaker, H.J.Aa. Jensen, P. Jørgensen, J. Olsen, H. Ågren, K.L. Bak, V. Bakken, P. Dahle, D. Jonsson, H. Heiberg, R. Kobayashi, H. Koch, K.V. Mikkelsen, P. Norman, K. Ruud, P.R. Taylor and O. Vahtras, DALTON, an ab initio electronic structure program.
[10] W.J. Hehre and W.A. Lathan, J. Chem. Phys. 56 (1972) 5255.
[11] R. Ditchfield, W.J. Hehre and J.A. Pople, J. Chem. Phys. 54 (1971) 724.
[12] J.J. Perez and H.O. Villar, Chem. Phys. Letters 188 (1992) 604.
[13] A. Hinchliffe and H.J.S. Machado, Chem. Phys. Letters 214 (1993) 64.
[14] E. Perrin, P.N. Prasad, P. Mougenot and M. Dupuis, J. Chem. Phys. 91 (1989) 4728.
[15] Y.-J. Lu and S.-L. Lee, Chem. Phys. 179 (1993) 431.
[16] P. Lazzeretti, M. Malagoli and R. Zanasi, Chem. Phys. Letters 167 (1990) 101.
[17] S. Heitz, D. Weidauer and A. Hese, Chem. Phys. Letters 176 (1991) 55.
[18] B.H. Ruessink and C. MacLean, J. Chem. Phys. 85 (1986) 93.
[19] M.F. Vuks, Opt. Spectry. 20 (1966) 361.
[20] P.J. Bounds and R.W. Munn, Chem. Phys. 24 (1977) 343.
[21] R.J.W. LeFevre and G.L.D. Ritchie, J. Chem. Soc. B (1968) 775.
[22] C.L. Cheng, D.S.N. Murthy and G.L.D. Ritchie, Australian J. Chem. 25 (1972) 1301.
[23] G.J.B. Hurst, M. Dupuis and E. Clementi, J. Chem. Phys. 89 (1988) 385.
[24] B. Kirtman, J. Toto, K. Robins and M. Hasan. J. Chem. Phys., 102 (1995) 5350.
[25] P. Norman, D. Jonsson, Y. Luo and H. Ågren, submitted for publication.